Iron-contamination-induced performance degradation of an iron-fed fuel cell

CrossMark

Min Sun [a, *], Wei Song [a], Lin-Feng Zhai [a], Zhong-Hua Tong [b]

[a] Department of Chemical Engineering, Hefei University of Technology, Hefei 230009, China
[b] Department of Chemistry, University of Science & Technology of China, Hefei 230026, China

HIGHLIGHTS

- Performance degradation of iron-fed fuel cell is attributed to iron contamination.
- Iron contaminant is presented in the form of α-FeO (OH).
- The α-FeO (OH) forms fouling layers on surfaces of electrode and membrane.
- The α-FeO (OH) migrates into the membrane to destroy the membrane structure.
- Electro-oxidation kinetics of Fe (II) is delayed by iron contamination.

GRAPHICAL ABSTRACT
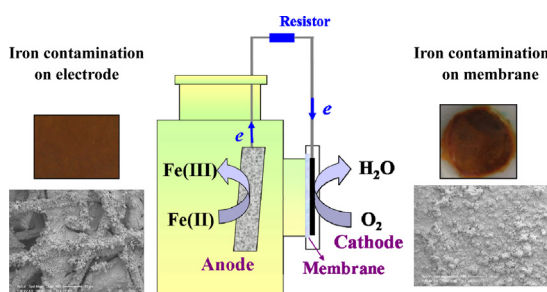
ARTICLE INFO

ABSTRACT

The iron-fed fuel cell is an effective technology to recover iron and electricity from acid mine drainage (AMD). However, this technology suffers from the problem of performance degradation which significantly reduces its power output during long-term operation. In this work, the performance degradation of iron-fed fuel cell is comprehensively evaluated with the objective to elucidate the mechanisms involved in such a phenomenon. The iron contamination is identified as the main cause responsible for the performance degradation of fuel cell. The iron contaminant is present in the form of α-FeO(OH), which is the main product recovered by the iron-fed fuel cell. Both the electrode and membrane are deteriorated by iron contamination, whereas the membrane deterioration is more significant. Fed-batch experiments demonstrate the performance loss of fuel cell due to contamination of membrane is more than 50% greater than the performance loss due to contamination of electrode. The α-FeO(OH) contaminant not only forms fouling layers on the surfaces of carbon electrode and membrane, but also migrates into the membrane to damage the membrane structure. As a result, both the charge transfer and mass transfer resistances of fuel cell are dramatically increased, which leads to delayed electro-oxidation kinetics of Fe(II).

1. Introduction

Acid mine drainage (AMD) is considered as the most serious and widespread mining industry related pollution problem around the word [1]. The AMD contains various dissolved heavy metals such as iron, aluminum, manganese and copper, among which the iron is of great interest with respect to recovery due to its high concentration

* Corresponding author. Fax: +86 551 2901450.
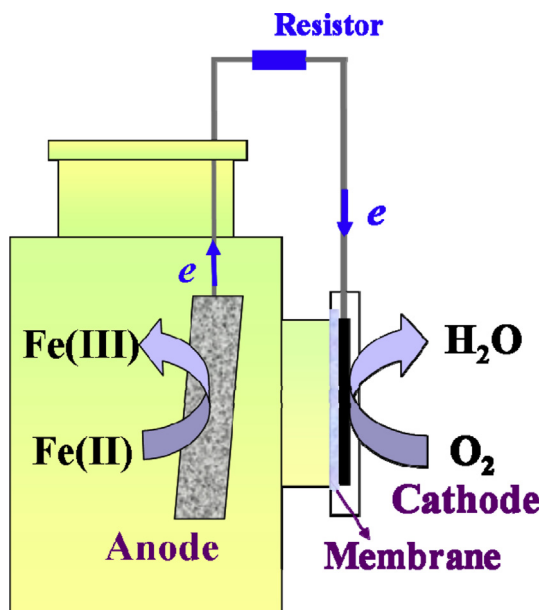 E-mail address: sunmin81@mail.ustc.edu.cn (M. Sun).

Fig. 1. Schematic diagram of the iron-fed fuel cell set up.

in AMD [2]. Recently, a novel air-cathode fuel cell technology has been proposed to selectively treat iron in the AMD [3,4]. The fuel cell system is composed of one anode chamber and one air-cathode which are separated by a membrane (Fig. 1). The ferrous ion (Fe(II)) can be spontaneously oxidized to the ferric (Fe(III)) state at the anode and the oxygen in the air is reduced to water at the cathode, with electricity concomitantly generated during the process. Since the Fe(II) is fed as substrate at the anode, this new type of fuel cell is denoted as iron-fed fuel cell. So far, the iron-fed fuel cell has been successfully operated with single-chamber and two-chamber fuel cell architectures [3,5]. The primary advantage of the iron-fed fuel cell is that it can effectively recover iron oxide and electricity from AMD under ambient condition. And the fact that zero emission is produced in the process makes this approach more favorable than other conventional AMD treatments.

Despite these many advantages, iron-fed fuel cell suffers from the problem of performance degradation which challenges its durability and reliability for application [5]. In fact, performance degradation has been frequently encountered in many fuel cell systems including polymer electrolyte membrane (PEM) fuel cells, microbial fuel cells and solid oxide fuel cells [6–9]. It is generally accepted that performance degradation can result from several causes, among which contamination by impurities is a very important factor affecting the performance of fuel cell. Works towards identifying the potential impacts of contamination on fuel cells classifies the contamination mechanisms into three major categories: 1) poisoning electrode catalysts, resulting in kinetic defect; 2) reducing conductivities including those of the membrane, electrolyte and electrode; and 3) modifying electrode structure and causing mass transfer problems [6]. Clearly it is necessary to obtain adequate knowledge about the nature and sources of contaminants, their impacts on the fuel cell performance and lifetime, and the mechanisms involved in the contamination if one wants to develop effective strategies to mitigate the adverse effects of contamination.

Iron represents one of the major potential contaminants towards fuel cell systems, which may lead to several types of performance losses including cathode and anode kinetic losses, ohmic loss, and mass transfer loss. Previous studies have shown even trace amount of iron in either Fe(II) or Fe(III) state significantly reduced the power output of PEM fuel cell due to the simple damage of membrane [10]. Since both the Fe(II) and Fe(III) are present in the iron-fed fuel cell which is operated with a PEM to separate the anode and cathode [5], it is presumed the iron contamination may play a role in the performance degradation of fuel cell.

As a recently developed technology, so far the iron-fed fuel cell has not been intensively studied, and the intrinsic mechanism involved in its performance degradation remains unclear. Therefore, the present work was undertaken with the objective to gain insight into the performance degradation of iron-fed fuel cell. The performance of fuel cell in long-time operation was evaluated in terms of the power output and charge-recovering ability. The role of iron as a potential contaminant was clarified and its fouling effect on the fuel cell components was elucidated. It is anticipated the results of this work would provide valuable information for the better control of the iron-fed fuel cell to produce more durable power from the AMD treatment.

2. Experimental

2.1. Construction and operation of the iron-fed fuel cell

The single-chamber iron-fed fuel cell was constructed as previously described [5], with the anodic volume of 175 mL. Both the anode and cathode were made from carbon paper and the cathode contained 0.05 mg cm^{-2} Pt catalyst on one side. The coated side of the cathode was positioned facing the GEFC-10N perfluorinated ion exchange membrane (4×4 cm^2, 0.254 mm of thickness, 0.1 S cm^{-1} of conductivity, GEFC Co., China) and the uncoated side was directly exposed to air. The projected surface areas of anode and cathode were 5 cm^2 and 4 cm^2, respectively. For the fuel cells operated in fed-batch mode, the anodic chamber was filled with deionized water containing 200 mM of NaCl as electrolyte and 50 mM of NaHCO$_3$ as pH buffer, and then sparged with a mixture of nitrogen (N$_2$) and carbon dioxide (CO$_2$) for 30 min to remove dissolved oxygen and to adjust solution pH to 8.2. The 0.14 M Fe(II) stock solution, which was prepared using FeSO$_4 \cdot$7H$_2$O, was added into the anodic chamber at 3.5 mM in an anaerobic glove box. The circuit of fuel cell was left open until a constant open circuit voltage was obtained, and then was connected with a 1 kΩ resistor. In the continuous-feed operation, the Fe(II)-fed medium stored in a 5 L oxygen-free container was pumped into the anodic chamber of fuel cell in an upflow mode at a constant flow rate of 0.125 mL min^{-1} through a peristaltic pump.

The voltage across the 1 kΩ external resistor was recorded at 10 min intervals using a data acquisition system (USB2801, ATD Co., China). The current was calculated using Ohm's law, and current density was then normalized by the projected surface areas of two sides of the anode (10 cm^2). The total number of recovered charges was calculated by integrating the current over time. Polarization curves were obtained on a CHI 660D electrochemical workstation (CH Instruments Inc., USA) by applying a linear potential decrease of 100 mV s^{-1} from the open circuit voltage to 0 mV.

2.2. X-ray diffraction (XRD) and scanning electron microscope (SEM) analyses on the iron contaminants

To obtain contaminated electrode and membrane samples for SEM and XRD analyses, three fuel cells were operated in fed-batch mode for one, two, and three batch cycles, respectively. Both the electrodes and membranes were maintained in the fuel cell until predetermined batch cycles were ended. In this way, electrodes and membranes were obtained which undergo one, two or three batch cycles.

Prior to analysis, part of the contaminated samples were cut into pieces and then dried at 60 °C. The surface structure and elemental components of the electrode and membrane were analyzed using a JSM-6700 SEM (JEOL Co., Japan) equipped with an energy dispersive X-ray spectrometry (EDX). The crystalline phase of the contaminant was identified by XRD using a Bruker D8 advance-X-ray diffractometer equipped with graphite-monochromated Cu Kα radiation (λ = 1.54178 Å).

2.3. Electrochemical impedance spectroscopy (EIS) with the contaminated electrode or membrane

EIS was carried out on a CHI 660D electrochemical workstation (CH Instruments Inc., USA) to characterize the electrochemical behavior of Fe(II) with contaminated carbon electrode or membrane. The samples were obtained from another three fed-batch fuel cells operated for one, two, and three batch cycles, respectively. The electrolyte solution contained 3.5 mM of Fe(II), 50 mM of NaHCO$_3$ and 200 mM of NaCl with solution pH of 8.2. For the carbon electrode, EIS was performed on a three-electrode assembly with the carbon paper as working electrode, platinum wire as counter electrode and saturated calomel electrode (SCE) as reference. For the membrane, EIS was performed on a one-chamber fuel cell with membrane electrode assembly (MEA). The MEA was prepared by firmly pressing the membrane onto a platinum foil (2 × 2 cm^2) which was used as both the counter and reference electrodes. A gold electrode (3 mm in diameter) was located in the anodic chamber of fuel cell as working electrode. The initial potential was set as the open circuit potential of working electrode under steady conditions, which was −0.518 V (vs. SCE) for the carbon electrode and 0.280 V (vs. SCE) for the gold electrode, respectively. The frequency of the AC signal was varied from 100 kHz to 0.01 Hz with potential amplitude of 5 mV. The electrolyte solution was purged with a mixture of N$_2$ and CO$_2$ for 30 min prior to EIS experiment, and a N$_2$/CO$_2$ environment was then maintained for the solution throughout the measurements. The ZView 2.0 software (Scribner Associates Inc., USA) was used to fit and simulate the impedance data.

2.4. Characterization of the membrane water uptake ability and ion exchange capacity (IEC)

The water uptake ability of membrane was evaluated by determining its water content as previously described [11]. At first the membrane was equilibrated in deionized water for 12 h at ambient temperature and then was weighed (W_{wet}). Next, the membrane was dried at 110 °C for 2 h and weighted again (W_{dry}). The water content was subsequently determined as (W_{wet} − W_{dry})/W_{dry} × 100%.

The IEC of the membrane was measured with titration method [7]. The membrane was firstly soaked in a 2.5 M NaCl solution for 10 h at ambient temperature to ensure the protons were replaced completely by the sodium ion. Then the NaCl solution was titrated against a 0.05 M NaOH solution to neutralize the exchanged protons using phenolphthalein as an indicator. After that, the IEC was calculated as:

$$IEC = \frac{a \times b}{W_{dry}} \tag{1}$$

where a is the added titrant volume at the equivalent point (mL), b is the molar concentration of the titrant (mmol mL^{-1}), and W_{dry} is the dry membrane weight (g). The values of the water content and IEC reported were the mean of five measurements.
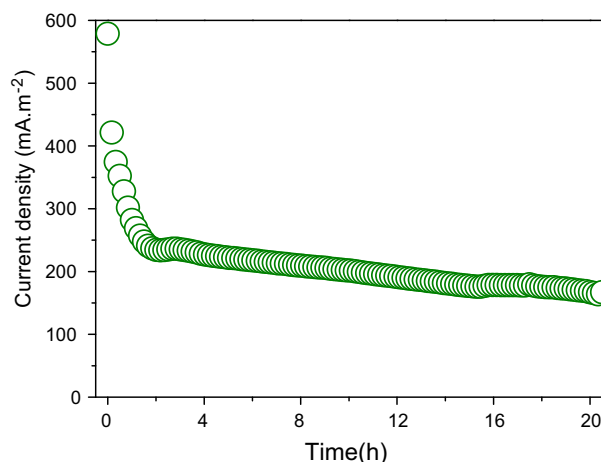

Fig. 2. Evolution of current density in the iron-fed fuel cell operated in continuous-feed mode.

3. Results and discussion

3.1. Current evolutions of the iron-fed fuel cell operated in continuous-feed mode and fed-batch mode

The potential of Fe(II) as a substrate to generate electricity was examined by monitoring the current evolution of a fuel cell operated in continuous-feed mode (Fig. 2). As soon as the circuit was closed, an instant current of 578 mA m^{-2} was generated which was rapidly dropped to 240 mA m^{-2} in 1.5 h. Then, current density was gradually declined until 170 mA m^{-2} in the next 20-hr of operation. Since the Fe(II) concentration maintained at 3.5 mM in continuous flow, it is concluded the current decay should be attributed to the performance degradation of fuel cell.

Next, one fuel cell (Fuel cell A) was operated in fed-batch mode and electricity generation in three complete sequential batch cycles was monitored (Fig. 3A). Due to the continuously reduced concentration of Fe(II) in anodic chamber, a current decline from the maximum to zero was observed within each batch cycle. However, electricity generation during the first cycle was significantly greater than those during the following two cycles. As listed in Table 1, the total number of charges recovered in the first cycle was calculated as 28.49 C, while it dramatically reduced by 47% to 15.23 C in the second cycle and further to 12.07 C in the third cycle. Fig. 4 shows the polarization and power density curves of the fuel cell obtained with fresh Fe(II)-fed medium at the end of each cycle. At the same anodic potential, current density was seriously decreased by orders of magnitude after three batch cycles. The maximum power output achieved as high as 165 mV m^{-2} as the fuel cell was initially started. In comparison, only 64 mV m^{-2} of maximum power remained after the first cycle of operation, which was further declined to merely 3.6 mV m^{-2} and 0.4 mV m^{-2} after the second and third cycles, respectively. These results demonstrated the performance of fuel cell was severely deteriorated in the fuel cell operation.

3.2. Ability losses of the electrode and membrane in the fuel cell operation

In terms of fundamental understanding, the performance degradation of fuel cell is mainly caused by ability loss of electrode or membrane [12]. Therefore, two fed-batch fuel cells were operated to investigate if the electrode or membrane were deteriorated in the operation. For the one fuel cell (Fuel cell B), the membrane was replaced with a new one at the end of each cycle while the
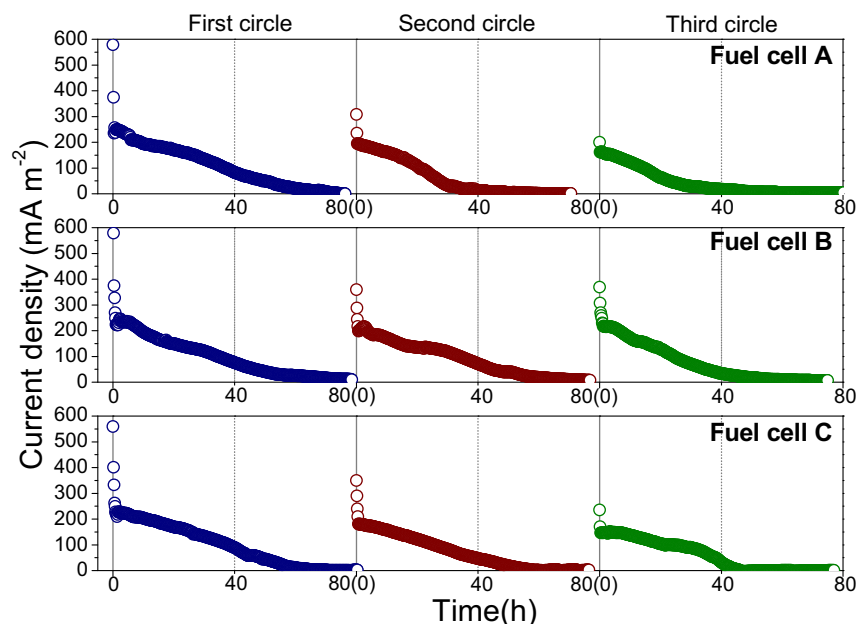
Fig. 3. Evolution of current density in Fuel cells A, B and C in three complete sequential fed-batch cycles. For Fuel cell B newly electrode is used at each cycle, and for Fuel cell C newly membrane is used at each cycle.

electrode was retained throughout the whole operation. For the other fuel cell (Fuel cell C), the electrode was replaced at each cycle while the membrane was retained. As shown in Fig. 3B and C, electricity generation was gradually attenuated from the first cycle to the third cycle in both fuel cells, suggesting the replacement of either electrode or membrane did not prevent performance degradation of fuel cell. It is thus deduced both the electrode and membrane were deteriorated in the operation of iron-fed fuel cell. Table 1 lists the numbers of total charges recovered by Fuel cells B and C over three sequential cycles. The charge-recovering ability of Fuel cell B was observed to lose by 11% at the second cycle and by 26% at the third cycle. The ability loss was more significant for Fuel cell C, which were 32% and 43% at the second and third cycles, respectively. Noticing that the performance degradation of Fuel cell A was more severe than performance degradations of Fuel cells B and C, it seems both the electrode and membrane deteriorations contributed to the performance degradation of iron-fed fuel cell. However, the membrane deterioration was more important to influence the performance of fuel cell, evidenced by the lower power output of Fuel cell C than that of Fuel cell B.

3.3. Characterizing the iron contaminants by XRD and SEM

The iron contaminants on the electrode and membrane were characterized by SEM and XRD. Fig. 5 demonstrates appearance changes of the electrode and membrane during three fed-batch cycles. The formation of red fouling layers (in web version) due to contamination is clearly observed on both the electrode and

membrane. And it seems the fuel cell contamination gradually aggravated from the first to the third cycle. The surface morphologies of electrode and membrane after three batch cycles were imaged using SEM. As shown in Fig. 6, the fouling layers consisted of granule-type substances which were identified as iron compounds by EDX (Supporting information, Figs. S1 and S2).

Fig. 7 shows the XRD patterns of electrode and membrane samples obtained in the fed-batch experiments. Bare carbon electrode displays two typical peaks located at 26.4° and 54.4°, which are assigned to the 002 and 004 facets of carbon (JCPDS 29-071341-1487). The characteristic peaks located at 21.3°, 33.2°, 34.7°, 36.7° and 53.3° clearly demonstrate the presence of α-FeO(OH) on the contaminated electrode [13], which had an orthorhombic phase with cell constants $a = 4.608$ Å, $b = 9.956$ Å, and $c = 3.022$ Å (JCPDS 29-0713). The peak intensities of α-FeO(OH) relative to peak intensities of carbon electrode are gradually enhanced from the first to the third cycle, implying more α-FeO(OH) crystals formed on the electrode. Similar peaks attributed to α-FeO(OH) are also observed on the XRD patterns of contaminated membrane, suggesting the α-FeO(OH) was the major product which caused contamination of both the electrode and membrane. This result is well consistent with previous study results which identified the α-FeO(OH) as the only product in the iron-fed fuel cell [3,4]. In analog to the case of electrode, XRD patterns demonstrate the membrane contamination was also aggravated from the first to the third batch cycle.

3.4. Clarifying key contributors to the performance degradation of fuel cell

The EIS is a powerful technique for the fuel cell diagnosis that provides information on the kinetics, mass transfer, and electrolyte and membrane resistances [14]. In order to characterize and differentiate the individual loss of electrode and membrane due to iron contamination, EIS was performed on the new and deteriorated electrodes and membranes. Accurate results of the resistances were obtained by fitting the impedance data to an equivalent electrical circuit illustrated in Figs. 8 and 9 [15,16]. In the equivalent electrical circuit, the constant phase element (C)

Table 1
Total charges (C) recovered in Fuel cells A, B and C during three sequential fed-batch cycles. For Fuel cell B newly electrode was used at each cycle, and for Fuel cell C newly membrane was used at each cycle.

|	First cycle	Second cycle	Third cycle
Fuel cell A	28.49	15.23	12.07
Fuel cell B (electrode replaced)	26.95	24.03	20.02
Fuel cell C (membrane replaced)	27.75	18.86	15.76
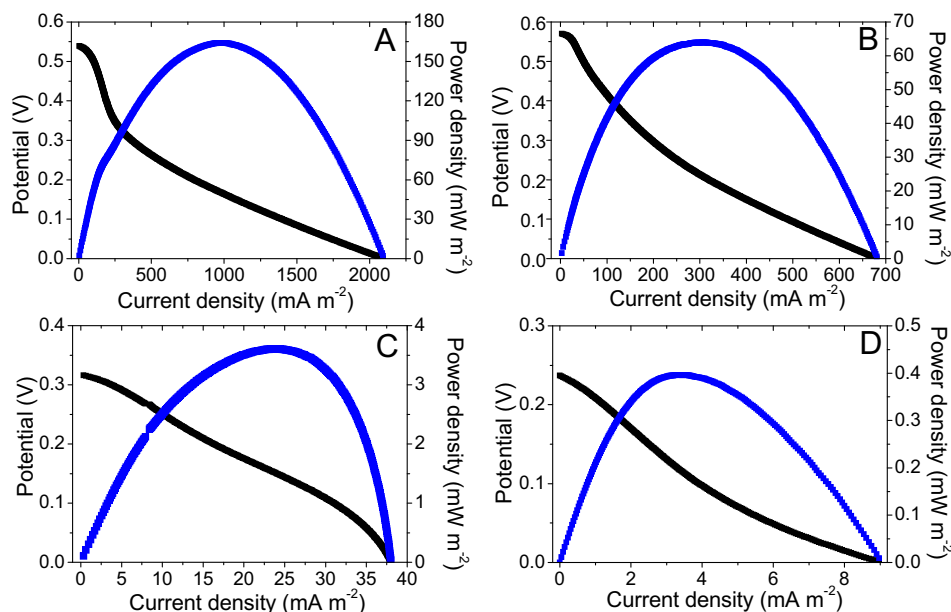
Fig. 4. Polarization and power density curves of the fuel cell with fresh Fe(II)-fed medium obtained A) before the first cycle; B) at the end of the first cycle; C) at the end of the second cycle; and D) at the end of the third cycle.

accounts for capacitance of the electrode and the Warburg element (Zw) represents a simple diffusion situation [17].

Fig. 8 shows the AC impedance spectrum in the Nyquist form obtained on the new and contaminated electrodes. At a very high frequency, the intercept at real part (Z′) represents an ohmic resistance (Rs) resulted from the ionic resistance of electrolyte, the intrinsic resistance of active materials and the contact resistance at the active material/current collector interface [15,18]. In this work, the Rs value can be used to evaluate the electrical conductivity of carbon electrode. Such a value was the lowest as 2.90 Ω for the new electrode, whereas doubled to 4.31 Ω for the electrode after one fed-batch cycle, suggesting the iron contamination greatly blocked electron transfer on the electrode. However, the Rs value was almost constant during the following two cycles, implying further formation of iron layers was of negligible influence on the conductivity of electrode. The diameter of semicircle on the Nyquist plot is equal to the charge-transfer resistance (Rct) at an electrode/electrolyte interface, which usually represents resistance of electrochemical reactions on the electrode [15,18]. The Rct was the lowest as 2.04 Ω for the new carbon electrode, indicating very fast electro-oxidation kinetics of Fe(II) on the electrode. This value jumped by 8 times—15.84 Ω on the electrode undergoing three running cycles, implying the electro-oxidation of Fe(II) on the electrode was sharply hindered by the iron contamination.

Fig. 9 shows the Nyquist plots obtained on the MEA with new and contaminated membranes. The intercept in the high-frequency domain, i.e. Rs, represents the membrane resistance from which the membrane through-plane conductivity under real fuel cell operating conditions can be measured [19]. The lowest Rs of 1.49 Ω was observed for the new membrane, yet such a value jumped to 96.88 Ω over the following three cycles of operation. This result demonstrates the ionic transport resistance across the membrane was significantly augmented by the iron contamination. The charge transfer resistance Rct represents the fuel cell reaction kinetics, which is determined by both the anodic Fe(II) oxidation process and cathodic oxygen reduction process. The Rct value rose by orders of magnitudes from 229 to 35,980 Ω after three running cycles, suggesting the iron contamination on the membrane severely retarded the fuel cell reaction kinetics. Note that the resistance on
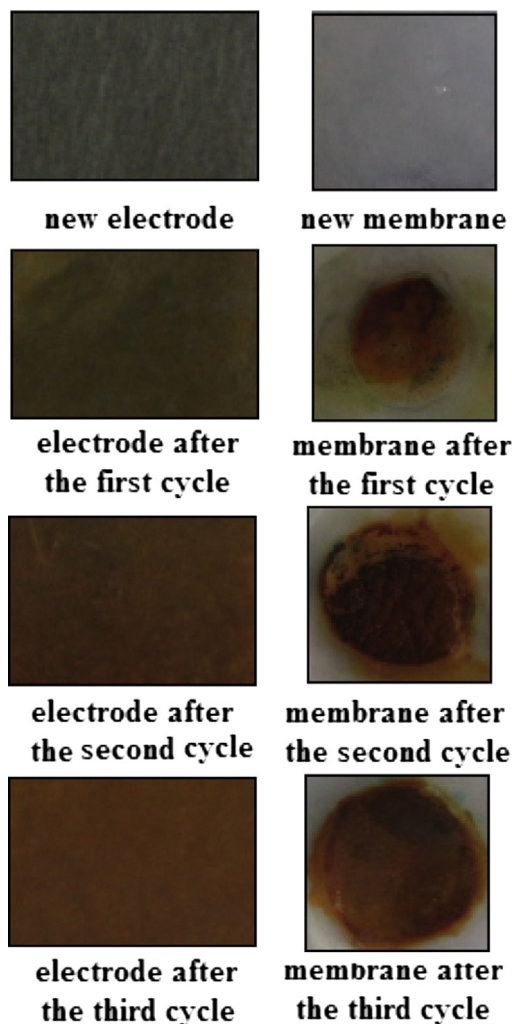
Fig. 5. Appearance changes of the electrode and membrane over three complete sequential fed-batch cycles.
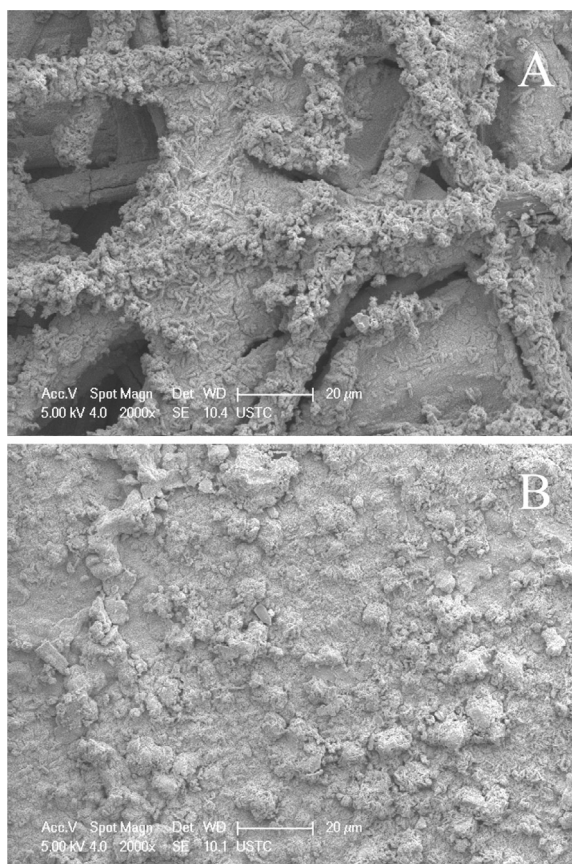
Fig. 6. SEM images of the A) contaminated electrode; and B) contaminated membrane.
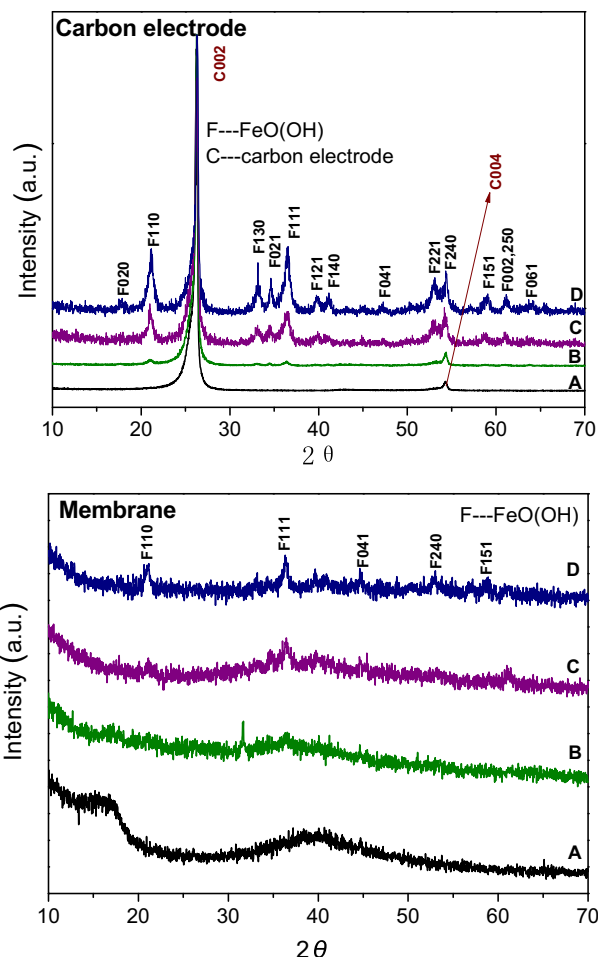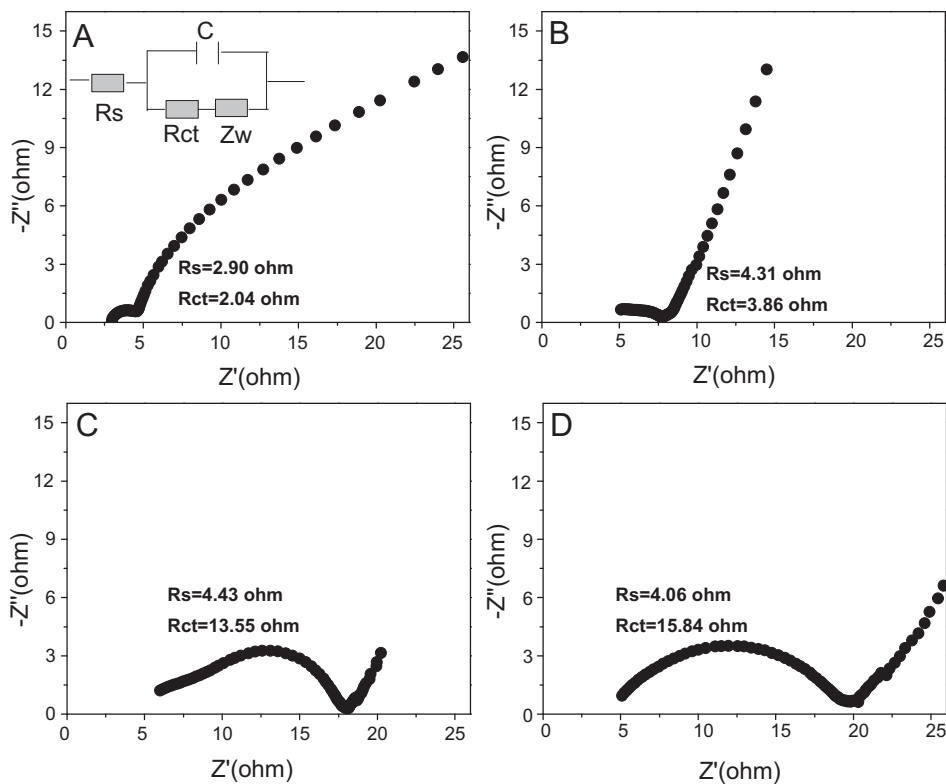

Fig. 7. XRD patterns of the electrode and membrane obtained A) before the first cycle; B) at the end of the first cycle; C) at the end of the second cycle; and D) at the end of the third cycle.

the electrode was substantially lower than that on the membrane, especially for the contaminated ones. It is thus concluded the membrane was the main component determining the total resistance of iron-fed fuel cell. Such a conclusion is also supported by our observation that electricity generation with contaminated membrane was lower than that with contaminated electrode (Fig. 3).

Both the charge transfer and mass transfer resistances of the fuel cell increased as a consequence of iron contamination. The increase of charge transfer resistance was mainly related to the delayed kinetics of cell reaction while the increase of mass transfer resistance was attributed to the decreased conductivity of membrane and electrode. Since the Rct was dramatically increased by orders of magnitude for the contaminated membrane, the significantly delayed oxidation kinetics of Fe(II) caused by membrane contamination is hence identified as the primary cause responsible for the performance degradation of iron-fed fuel cell. For the single-chamber iron-fed fuel cell, oxygen diffused through the membrane might oxidize the Fe(II) but without electricity generation [20]. As the electro-oxidation of Fe(II) on the electrode was hindered, more Fe(II) was consumed by the oxygen which led to decreased power output of the fuel cell.

3.5. Elucidating mechanisms involved in the iron contamination to the electrode and membrane

To help understand mechanisms involved in the iron contamination, the contaminated electrode and membrane from Fuel cell A were treated in 0.1 M of HCl solution for 12 h to dissolve the α-FeO(OH) on their surface and then rinsed with deionized water.

Next, two fuel cells (Fuel cell D and Fuel cell E) were operated with Fuel cell D composed of HCl-treated electrode and new membrane while Fuel cell E composed of new electrode and HCl-treated membrane. Power out of Fuel cell D was close to that of fuel cell with new electrode and membrane, suggesting the electrode performance was readily recovered by removing the surface fouling layers. Power out of Fuel cell E, however, was visibly lower than that with new electrode and membrane (Supporting information, Fig. S3). It is thus presumed other mechanisms would involve in the iron contamination to membrane besides forming surface fouling layers.

In order to go deep into the membrane contamination mechanisms, SEM was conducted on the cross-section of contaminated membrane after HCl treatment (Fig. 10A and B). Compared to the plain morphology displayed by cross-section of new membrane, the cross-section of HCl-treated membrane was much rougher with twisted structure and several micro-scale pinholes. The EDX analysis detected iron compound within the HCl-treated membrane, which was clarified as α-FeO(OH) by XRD (Supporting information, Figs. S4 and S5). These results suggested the α-FeO(OH) could migrate into the membrane and change the membrane structure.

The contaminated membrane after HCl treatment was further immersed in 1 M of H_2SO_4 solution for 2 h at 80 °C to fully yield H^+ form of membrane [21], and then the water uptake ability and IEC of membrane were investigated to evaluate the membrane

Fig. 8. Nyquist plots with the electrode obtained A) before the first cycle; B) at the end of the first cycle; C) at the end of the second cycle; and D) at the end of the third cycle. The inset in A) illustrates the equivalent circuit used to fit the EIS.

property. As shown in Fig. 10C, the membrane cross-section did not recover after H_2SO_4 treatment, suggesting the membrane structure was irreversibly damaged by iron contamination. The water content of the H_2SO_4-treated membrane was determined as 26.83 ± 2.31 wt.%, which was 11% lower than the 30.28 ± 2.21 wt.% of water content for new membrane. Meanwhile, the IEC of H_2SO_4-treated membrane significantly declined to 0.99 ± 0.08 mmol g^{-1} compared to the 1.17 ± 0.05 mmol g^{-1} value obtained on new ones.
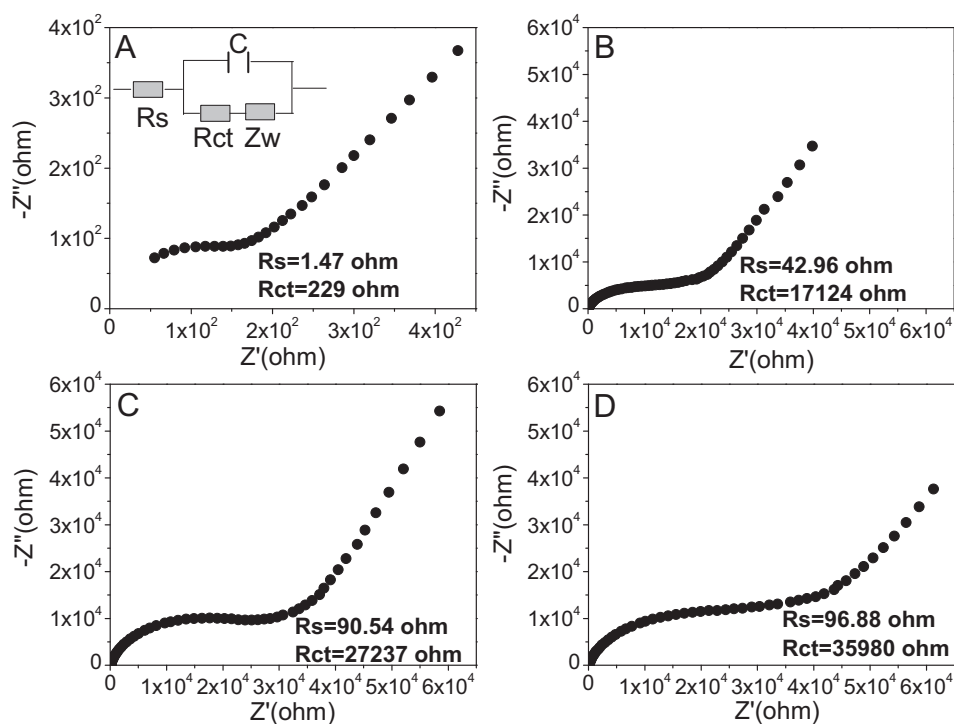
Fig. 9. Nyquist plots with the membrane obtained A) before the first cycle; B) at the end of the first cycle; C) at the end of the second cycle; and D) at the end of the third cycle. The inset in A) illustrates the equivalent circuit used to fit the EIS.
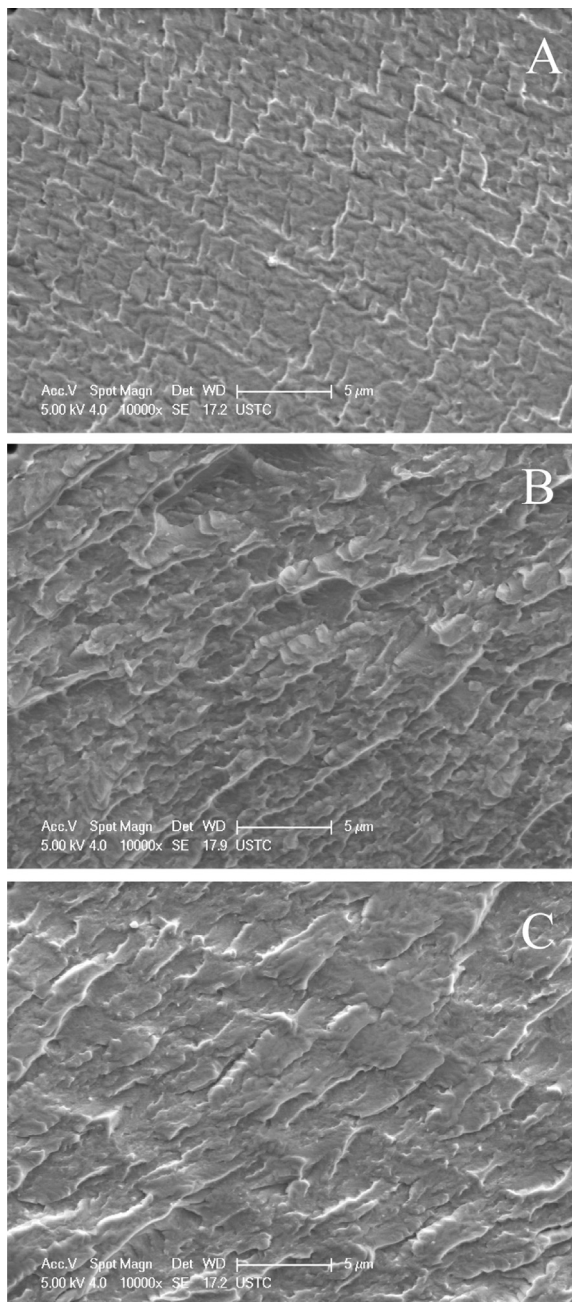
Fig. 10. SEM images of the cross-sections of A) new membrane; and B) contaminated membrane after treated by 0.1 M of HCl solution; and C) contaminated membrane after treated by 0.1 M of HCl and 1 M of H_2SO_4 solutions.

The decreased water uptake ability and IEC implied the membrane property was deteriorated as a result of structure damage.

3.6. Significance of this work

The iron-fed fuel cell is not only promising in treating the AMD, but also can be applied in other waste treatments such as desulfurization process to recover energy from wastes [22]. However, the iron contamination causes performance degradation of such a device, with the result that the power output of the fuel cell is impaired. Therefore, developing strategies that effectively control the iron contamination is one of the most important issues in the fuel cell application to ensure sustainable electricity production. In this work, we elucidate the mechanism involved in the iron contamination, thus providing valuable information for the better control of iron-fed fuel cell to mitigate the problem of performance degradation.

The iron-fed fuel cell is able to effectively recover iron from AMD in the form of α-FeO(OH) [3,4]. However, the produced α-FeO(OH) can precipitate or be absorbed on the electrode, thereby forming fouling layers on the its surface. Although previous study claimed the iron oxides were conductive and would not significantly influence the conductivity of electrode [3], our results have demonstrated undoubtedly the electro-oxidation of Fe(II) on the electrode is hindered by the fouling layer. Reasons of such an adverse effect may be attributed to the coverage and blockage of fouling layer to the carbon surface. At the conductive end planes of carbon are spread many functional groups such as carboxylic acids, alcohols, and quinones [15,23]. The α-FeO(OH) can interact with these functional groups and occupy a substantial portion of the electro-active sites. Moreover, the fouling layer covering the electrode surface blocks the porous structure of carbon paper (Fig. 6A), thus restricting the diffusion of Fe(II) into these pores. As a result, the surface area available for Fe(II) oxidation is reduced. The formation of α-FeO(OH) layers on the electrode not only diminishes the power out of fuel cell, but also brings difficulty to the recovery of α-FeO(OH) product. Therefore, measures aiming at minimizing affinity between α-FeO(OH) and the electrode should be pursued in the future to avoid electrode contamination from the aspect of both iron and energy recoveries.

In addition, the iron-fed fuel cell suffers from serious membrane deterioration caused by iron contamination. The α-FeO(OH) not only forms blocking layers on the membrane surface to prevent ion transfer, but also migrates into the membrane to damage the membrane structure. The water uptake ability of membrane would be reduced by the α-FeO(OH) intruding into the membrane polymer network, thus inducing conductivity loss of the membrane [11]. Moreover, the α-FeO(OH) decreases ionic exchange capacity of membrane, further lowering the membrane conductivity. Since the iron contamination irreversibly deteriorates the membrane and causes significant performance degradation of the iron-fed fuel cell, anti-fouling membrane with high resistance to the iron contamination should be developed to ensure a long-term stable operation of the fuel cell.

The significance of this work is not limited to the iron-fed fuel cell, but is extended to a wide range of PEM fuel cells. Insufficient durability and reliability caused by performance degradation is one of the greatest technical barriers for the commercialization of PEM fuel cells. Iron is a usually encountered metal impurity which shows detrimental effect on the performance of PEM fuel cells. Previous studies usually attributed such adverse effect to the membrane degradation caused by iron ions [6]. In this work, we demonstrate the corrosion of carbon electrode by iron compounds can also result in performance degradation of PEM fuel cell. Specifically, we for the first time show that the electrochemical transformation of Fe(II) to Fe(III) on the electrode plays a significant role in the iron contamination. These findings have enriched our understanding about the iron contamination.

4. Conclusions

The iron-fed fuel cell suffers from the problem of performance degradation which is caused by iron contamination on both electrode and membrane. The iron contaminant is present in the form of α-FeO(OH), which is the product recovered from the iron-fed fuel cell. Although both the electrode and membrane contaminations contribute to the performance degradation of iron-fed fuel cell, the membrane contamination is more significant to increase the total resistance in the fuel cell. The contamination mechanisms of iron

on the electrode and membrane were quite different. The α-FeO(OH) can form fouling layers on the surface of electrode, thereby hindering the electro-oxidation of Fe(II). Such a compound, however, is found to migrate into the membrane to destroy its structure besides forming surface fouling layers on the membrane. As a result, the membrane conductivity is significantly augmented which leads to delayed electro-oxidation kinetics of Fe(II).

Acknowledgments

Appendix A. Supplementary data

Supplementary data related to this article can be found at http://dx.doi.org/10.1016/j.jpowsour.2013.09.057.

References

[1] C.M. Neculita, G.J. Zagury, B. Bussiere, J. Environ. Qual. 36 (2007) 1–16.
[2] S.L.F. Andersen, R.G. Flores, V.S. Madeira, H.J. Jose, R.F.P.M. Moreira, Ind. Eng. Chem. Res. 51 (2012) 767.
[3] S. Cheng, B.A. Dempsey, B.E. Logan, Environ. Sci. Technol. 41 (2007) 8149.
[4] S. Cheng, J.H. Jang, B.A. Dempsey, B.E. Logan, Water Res. 45 (2011) 303.
[5] L.F. Zhai, Z.H. Tong, M. Sun, W. Song, S. Jin, H. Harada, Ind. Eng. Chem. Res. 52 (2013) 2234–2240.
[6] X. Cheng, Z. Shi, N. Glass, L. Zhang, J. Zhang, D. Song, Z.S. Liu, H. Wang, J. Shen, J. Power Sources 165 (2007) 739–756.
[7] J. Xu, G.P. Sheng, H.W. Luo, W.W. Li, L.F. Wang, H.Q. Yu, Water Res. 46 (2012) 1817–1824.
[8] H. Li, K. Tsay, H. Wang, J. Shen, S. Wu, J. Zhang, N. Jia, S. Wessel, R. Abouatallah, N. Joos, J. Schrooten, J. Power Sources 195 (2010) 8089–8093.
[9] H. Yokokawa, K. Yamaji, M.E. Brito, H. Kishimoto, T. Horita, J. Power Sources 196 (2011) 7070–7075.
[10] M. Sulek, J. Adams, S. Kaberline, M. Ricketts, J.R. Waldecker, J. Power Sources 196 (2011) 8967–8972.
[11] H. Beydaghi, M. Javanbakht, H.S. Amoli, A. Badiei, Y. Khaniani, M.R. Ganjali, P. Norouzi, M. Abdouss, Int. J. Hydrogen Energy 36 (2011) 13310–13316.
[12] W. Schmittinger, A. Vahidi, J. Power Sources 180 (2008) 1–14.
[13] Y. Ni, X. Ge, H. Liu, Z. Zhang, Q. Ye, F. Wang, Mater. Lett. 49 (2001) 185–188.
[14] X.Y. Yuan, H. Wang, J.C. Sun, J. Zhang, Int. J. Hydrogen Energy 32 (2007) 4365–4380.
[15] M. Sun, F. Zhang, Z.H. Tong, G.P. Sheng, Y.Z. Chen, Y. Zhao, Y.P. Chen, S.Y. Zhou, G. Liu, Y.C. Tian, H.Q. Yu, Biosens. Bioelectron. 26 (2010) 338–343.
[16] Y. Qiao, C.M. Li, S.J. Bao, Q.L. Bao, J. Power Sources 170 (2007) 79–84.
[17] Z. He, F. Mansfeld, Energy Environ. Sci. 2 (2009) 215–219.
[18] A.J. Bard, L.R. Faulkner, Electrochemical Methods: Fundamentals and Applications, second ed., Wiley, New York, 2001.
[19] J. Zhang, L. Zhang, C.W.B. Bezerra, H. Li, Z. Xia, J. Zhang, A.L.B. Marques, E.P. Marques, Electrochim. Acta 54 (2009) 1737–1743.
[20] H. Liu, B.E. Logan, Environ. Sci. Technol. 38 (2004) 4040–4046.
[21] C.H. Wan, C.L. Chen, Int. J. Hydrogen Energy 34 (2009) 9515–9522.
[22] L.F. Zhai, W. Song, Z.H. Tong, M. Sun, J. Hazard. Mater. 243 (2012) 350–356.
[23] S.R. Crittenden, C.J. Sund, J.J. Sumner, Langmuir 22 (2006) 9473–9476.